ACS Catalysis

Research Article

pubs.acs.org/acscatalysis

Construction of Graphitic C_3N_4-Based Intramolecular Donor–Acceptor Conjugated Copolymers for Photocatalytic Hydrogen Evolution

Xiangqian Fan, Lingxia Zhang,* Ruolin Cheng, Min Wang, Mengli Li, Yajun Zhou, and Jianlin Shi*

State Key Laboratory of High Performance Ceramics and Superfine Microstruture, Shanghai Institute of Ceramics, Chinese Academy of Sciences, 1295 Ding-xi Road, Shanghai 200050, People's Republic of China

Supporting Information

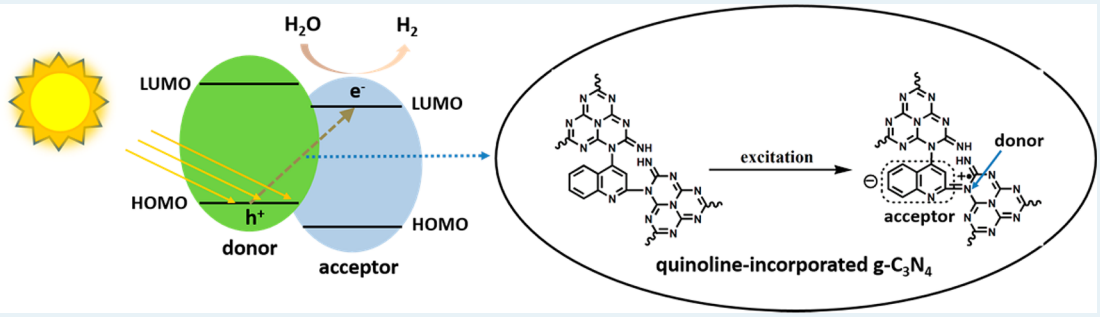

ABSTRACT: The construction of intramolecular donor–acceptor conjugated copolymers has been devised for years to enhance the mobility of charge carriers in an organic photovoltaic field; however, surprisingly, similar strategies have not been reported in polymeric photocatalytic systems for promoting the separation of charge carriers. Graphitic carbon nitride ($g\text{-}C_3N_4$) is an emerging polymeric visible-light photocatalyst with high stability but still low photocatalytic efficiency. Here, we prepared a series of $g\text{-}C_3N_4$-based intramolecular donor–acceptor copolymers (aromatics-incorporated $g\text{-}C_3N_4$) via nucleophilic substitution/addition reactions. The copolymer showed remarkably enhanced and stable visible-light photocatalytic hydrogen evolution performance. The intramolecular charge transfer transition is first proposed to explain the photocatalytic activity of $g\text{-}C_3N_4$-based photocatalysts under long-wavelength-light irradiation.

KEYWORDS: *$g\text{-}C_3N_4$, copolymerization, donor–acceptor, photocatalysis, water splitting*

1. INTRODUCTION

A sustainable clean energy supply is urgently needed nowadays because of the gradual depletion of fossil fuels. Among diverse renewable energy sources, solar energy is considered the most prospective one.[1] Converting it into chemical and electric energy by photocatalytic and photovoltaic devices, respectively, is two of the basic ways to store it for further use,[2] but how to capture and convert solar energy efficiently remains a big challenge. As a kind of burgeoning light conversion material in the past few decades, conjugated polymer semiconductors make a conspicuous figure in solar energy industries because of their simple manufacture, low cost, light weight, flexibility, etc.,[3] compared with conventional inorganic semiconductors.[4] One major factor that determines the energy conversion efficiency of conjugated polymer semiconductors is the lifetime of the excitons.[5] It is known that in conjugated donor–acceptor (DA) systems, an intramolecular charge transfer that results in the effective separation of charge carriers will take place under irradiation.[6] Recently, in the organic photovoltaic field, various intramolecular DA copolymers have been developed to elevate the mobility of charge carriers.[7] It is reasonable to predict that these conjugated DA systems may also be effective and applicable in the polymeric photocatalytic field, which, however, to our surprise, has not been reported as far as we could find.

Graphitic carbon nitride ($g\text{-}C_3N_4$) is a polymeric visible-light photocatalyst attracting much attention in recent years (Figure S1).[8] Compared with well-established polymeric photocatalysts,[9] $g\text{-}C_3N_4$ features facile preparation, higher thermo-/chemical stability, and photocatalytic efficiency. Unfortunately, like most of the polymeric photocatalysts, photogenerated carriers in $g\text{-}C_3N_4$ have poor mobility.[3d,10] To promote the separation efficiency of charge carriers, the most common method is to construct heterojunctions between the interface of the $g\text{-}C_3N_4$ and other semiconductors.[11] However, in conventional complexes with interfacial heterojunctions, only those charge carriers located around the phase interface can be separated effectively, and it is still unavoidable that a large proportion of charge carriers will recombine with each other before they are transported to the heterojunction interface, leading to limited enhancement of the photocatalytic efficiency.

Received: June 4, 2015
Revised: July 16, 2015
Published: July 17, 2015

DOI: 10.1021/acscatal.5b01155
ACS Catal. 2015, 5, 5008–5015

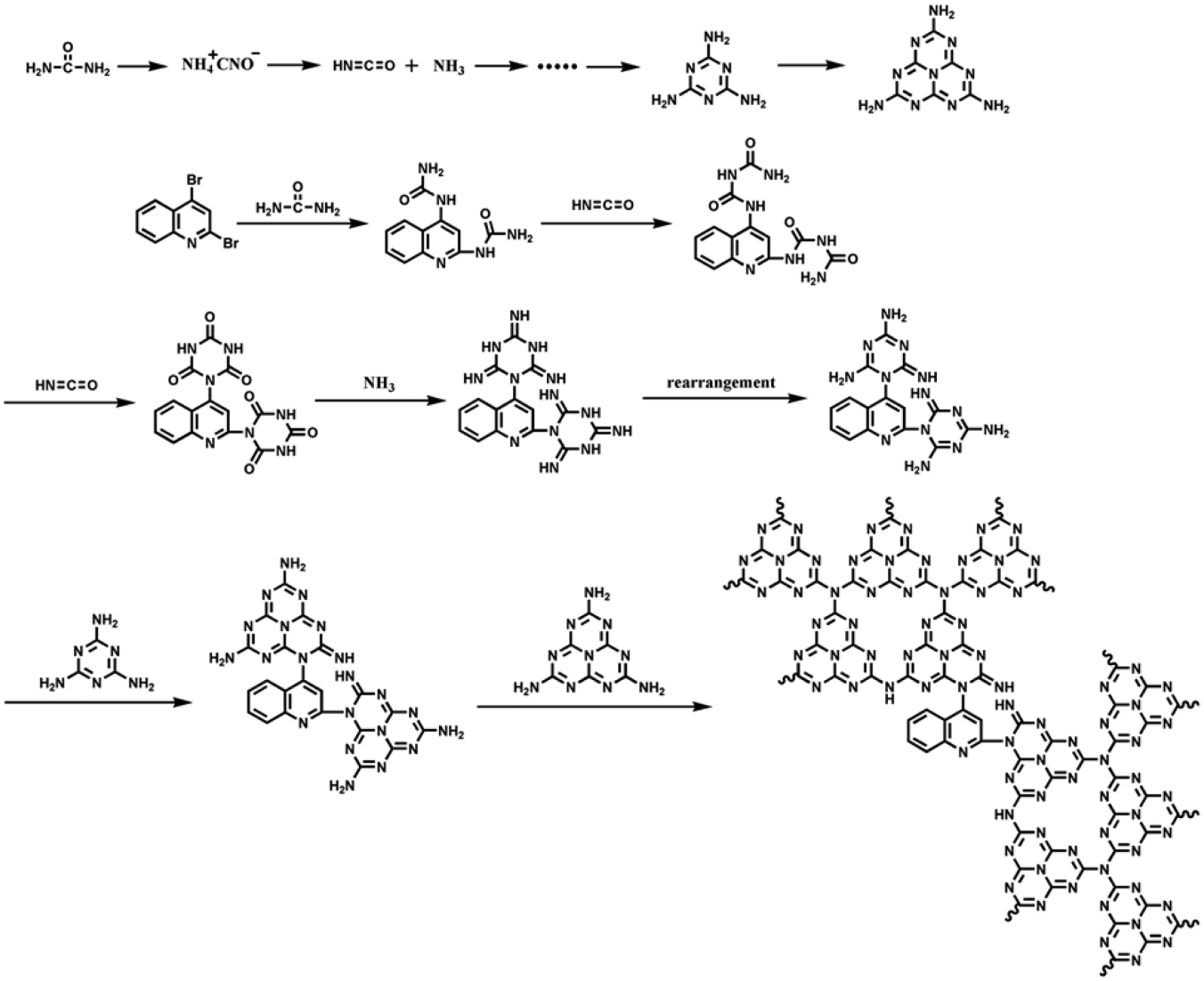

Figure 1. Possible reaction path of incorporating quinoline into g-C_3N_4 networks.

Inspired by the intramolecular DA copolymers, which have been applied in photovoltaic technology, it is expected that introducing appropriate donor or acceptor units into g-C_3N_4 networks would facilitate the separation of charge carriers and elevate the photocatalytic performance. Herein, a series of dibromo aromatics have been chosen as the comonomers to react with urea (the precursor to the synthesis of g-C_3N_4 with best photocatalytic performance[12]), which has nucleophilic amino groups, to construct novel intramolecular DA copolymers for photocatalytic application. It is worth noting that the strategy presented in this work is different from the well-established copolymerization method that has been applied in modifying g-C_3N_4.[13] The comonomers selected in our strategy acted as nucleophilic substitution substrates, which are different from those in previous methods and used as nucleophilic addition substrates. This leads to the structural difference between the final copolymers: In our strategy, the aromatic rings are connected by adjacent 3,s-triazine units, whereas in the previous report, they are incorporated into the inner 3,s-triazine units.

2. EXPERIMENTAL SECTION

2.1. Materials. Urea (>99%) was purchased from Sinopharm Chemical Reagent Co., Ltd.; 2,4-dibromoquinoline (>97%), 2,5-dibromopyrimidine (>98%), triethanolamine (>97%), and chloroplatinic acid hexahydrate (>%37.5, Pt basis) were purchased from Sigma-Aldrich Co., LLC.; 2,4-dibromopyridine (>98%) was purchased from Adamas Reagent, Ltd.; 1,4-dibromobenzene (>99%) was purchased from TCI Co., Ltd.

2.2. Synthetic Procedures. In a typical synthesis procedure, 20 g of urea and a certain amount of dibromo aromatic compounds were mixed thoroughly, and then the mixture was put into an alumina crucible with a cover and heated to 550 °C for 2 h at a heating rate of 5 °C/min. After undergoing various reactions at high temperature, the as-constructed copolymer based on g-C_3N_4 and aromatics was obtained.

2.3. Characterization. The X-ray diffraction (XRD) patterns were recorded on a RigakuUltima IV diffractometer. Fourier transform infrared (FT-IR) spectra were obtained using a Nicolet iS10 FTIR spectrometer. High-resolution FT-IR spectra were conducted on Nicolet Avatar 330 FTIR

DOI: 10.1021/acscatal.5b01155
ACS Catal. 2015, 5, 5008−5015

spectrometer. X-ray photoelectron spectroscopy (XPS) measurements were carried out on a Thermo Scientific Escalab 250 spectrometer with Al Kα radiation as the excitation source. Binding energies for the high-resolution spectra were calibrated by setting C 1s to 284.6 eV. Transmission electron microscopy (TEM) images and electron energy loss spectroscopy (EELS) results were obtained with a FEI Magellan 400 instrument. The textural parameters (surface area, pore volume, pore width) were measured using a Micromeritics TriStar 3000 system. Elemental analysis (C, H, N) was taken on a vario EL cube microanalyzer. UV−vis diffuse reflectance spectra were performed on a Shimadzu UV-3600 system. Photoluminescence (PL) spectra and fluorescence lifetime spectra were recorded at room temperature with a fluorescence spectrophotometer (Edinburgh Instruments, FLSP-920). The excitation wavelength was 380 nm. Electron paramagnetic resonance (EPR) measurements were performed on a Bruker EMX-8/2.7 spectrometer.

2.4. Electrochemical Analysis. Electrochemical measurement were conducted with a CHI 760 electrochemical workstation in a conventional three electrode cell using a Pt plate and a Ag/AgCl electrode as counter electrode and reference electrode, respectively. Working electrodes were obtained by transferring photocatalyst suspensions (10 mg in 3 mL ethanol) onto FTO conductive glass using a spin-coating method, and the electrodes were annealed at 150° for 2 h. A 0.2 M Na_2SO_4 aqueous solution was chosen as the supporting electrolyte and was purged with nitrogen to remove O_2 before any measurements. The visible light was generated by a 300 W Xe lamp with 420 nm and IR cutoff filters and was chopped manually.

2.5. Photocatalytic Hydrogen Evolution Test. The photocatalytic reactions were carried out in a quartz reaction vessel connected to a closed gas circulation and evacuation system. A 0.1 g portion of catalyst was suspended in 100 mL of aqueous solution containing triethanolamine (10 vol %) as the sacrificial electron donor. Three weight percent Pt was loaded onto the surface of the catalyst by an in situ photodeposition method using $H_2PtCl_6{\cdot}6H_2O$ as precursor. The suspension was thoroughly degassed and irradiated by a 300 W Xe lamp equipped with an optical UV-IR cutoff filter (780 nm > λ > 420 nm) to eliminate UV and IR light. The temperature of the reactant solution was maintained at 283 K by a flow of cooling water during the reaction. The evolved gas was analyzed every 1 h by gas chromatography equipped with a thermal conductive detector. For a stability test, the system was evacuated every 4 h and repeated 4 times (i.e., a 16 h recycling experiment with intermittent evacuation every 4 h). The apparent quantum yield (AQY) for H_2 evolution was measured using the 420, 450, 500, 550, 600, and 650 nm band-pass filter. The average intensity of irradiation was measured by a Coherent Fieldax-TO spectroradiometer. The AQY was estimated as

$$\text{AQY}\ (\%) = \text{number of evolved } H_2\text{molecules} \times 2 \times 100/\text{number of incident photons}$$

3. RESULTS AND DISCUSSION

For quinoline incorporated copolymers, we denote them as CNQ-*X*, where *X* (g) represents the amount of 2,4-Dibromo quinoline added. The possible reaction mechanism is proposed in Figure 1. As indicated, the incorporated quinoline rings are located at the terminals of the copolymer.

The XRD patterns and FT-IR spectra (Figure S2a,b, respectively) of CNQ-*X*s show all the characteristic peaks of pure g-C_3N_4 (denoted as CN). With more quinoline rings being incorporated, both XRD and FT-IR peaks become weaker and broadened. This indicates that the incorporation of quinoline rings into g-C_3N_4 networks can alter its chemical environment and deteriorate the periodicity of the g-C_3N_4 layers/network to some extent, but its main chemical skeleton has been retained. It is worth noting that, as shown in the FT-IR spectra, pure g-C_3N_4 (CN) exhibits an absorption peak at ~2349 cm^{-1} belonging to the adsorbed CO_2 molecules,[12b] but CNQ-*X* does not. This can be attributed to the fact that the incorporated quinoline rings are located at the terminals of the copolymers, leading to the decreased density of terminal $-NH_2$ groups for anchoring CO_2 molecules. High resolution FT-IR spectra were recorded for samples CN and CNQ-0.03 (Figure 2). Compared with CN, CNQ-0.03 exhibits a distinguishable IR

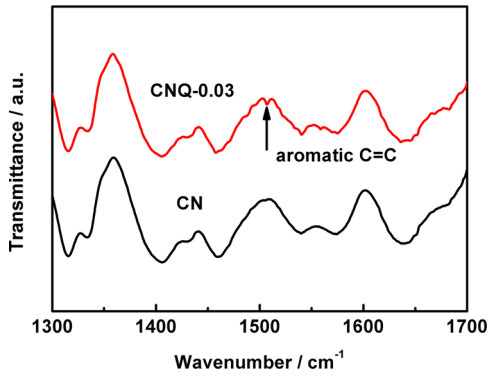

Figure 2. High-resolution FT-IR spectra of CN and CNQ-0.03.

band located at 1507 cm^{-1}, and the strongest IR peak of quinoline is located just right at ~1500 cm^{-1} (attributed to aromatic C=C) according to a previous report.[14] As far as we know, 2,4-dibromoquinoline cannot polymerize by itself. So considering the low amount of 2,4-dibromo quinoline added, it can be preliminarily concluded that quinoline rings have been successfully incorporated into g-C_3N_4 networks.

Table S1 gives the elemental analysis results of all the samples. It is expected that if quinoline can be successfully incorporated into g-C_3N_4 networks, the C/N ratio and H content of the polymer will increase with more quinoline rings being incorporated. The results agree well with this expectation. Note that the C/N ratio in CN is higher than CNQ-(0.01−0.05), which is due to its high carbon content resulting from surface-adsorbed CO_2, as demonstrated by the FT-IR spectra. The detailed chemical composition and structure features of CN and CNQ-0.03, as a representative of CNQ-*X*s, were revealed by XPS analysis. As shown in Figure S3, only three signals belonging to C, N, O can be found in CNQ-0.03, proving that Br has been eliminated thoroughly in the polymerization process. The weak O signal may arise from the adsorbed oxygen-containing adventitious contaminants.[12a] High-resolution spectra of C 1s and N 1s were measured to further confirm the presence of carbon and nitrogen species (Figure S3). CNQ-0.03 shows all the representative C and N peaks of CN. In addition, another peak centered at 398.9 eV is observed in the N 1s spectrum of CNQ-0.03, which can be assigned to terminal C=NH groups.[15]

Figure 3 shows typical TEM images of CN, CNQ-0.03, and CNQ-0.50. CN exhibits layered platelet morphology, whereas

DOI: 10.1021/acscatal.5b01155
ACS Catal. 2015, 5, 5008−5015

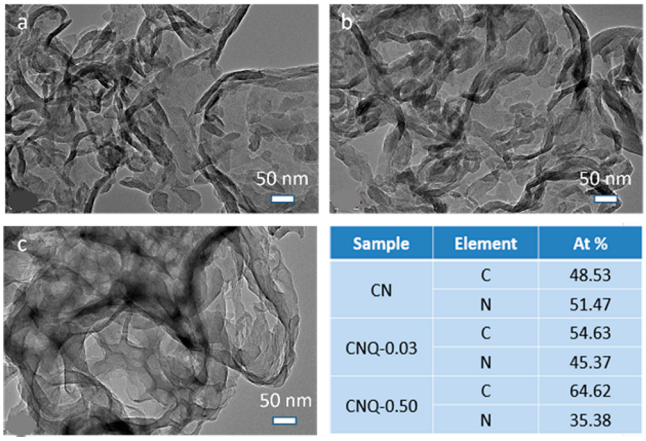

Sample	Element	At %
CN	C	48.53
	N	51.47
CNQ-0.03	C	54.63
	N	45.37
CNQ-0.50	C	64.62
	N	35.38

Figure 3. Typical TEM images of (a) CN, (b) CNQ-0.03, and (c) CNQ-0.50. The table at bottom right summarizes the EELS elemental analysis results conducted at the edge of the lamellas of these samples.

after quinoline incorporation, a curved/distorted structure dominates. The EELS spectra were recorded at the particle edges of these copolymers, where quinoline rings are located. Not surprisingly, the atomic C/N ratio was found to increase with the increasing added amount of quinoline rings. The pore-related textural parameters and pore size distribution of CN and CNQ-*X*s are presented in Table S2 and Figure S4, respectively. It can be seen that a proper amount of incorporation of quinoline rings has resulted in an increased BET surface area, pore volume, and pore size, whereas excessive addition led to decreases in these parameters. This can be attributed to the inhibition effect of the incorporated quinoline rings on the polymerization of 3,s-triazine rings which causes a certain degree of distortion to carbon nitride networks. As for the moderately distorted structure, pores can be formed/enlarged because of the twisting and folding of carbon nitride networks; however, excess distortion of carbon nitride networks would lead to pore structure collapse of the copolymers.

Figure 4a shows the UV−vis absorption spectra of CN and CNQ-*X*s. Obviously, with the increasing amount of quinoline ring incorporation, the absorption gets stronger almost throughout the whole wavelength range, which demonstrates that quinoline incorporation would considerably enlarge the delocalization range of the electrons in g-C_3N_4 networks. This can be confirmed by the electron paramagnetic resonance (EPR) spectra of CN and CNQ-*X*s (Figure S5). A classical Tauc approach[16] was applied to estimate the optical band gap of as-prepared samples (Figure S6, Table S2). The overall trend is that the copolymer incorporated with the larger number of quinoline rings shows basically the narrower band gap. According to their UV−vis absorption spectra with more and more obvious "shoulder"- and "tail"-like features in the visible light region, we can see that an additional electron-transition mode gradually appears, except the electron transition from intrinsic HOMO to LUMO.[17] Considering the structure of these copolymers, the intramolecular charge transfer transition will most probably occur in it.

Charge transfer transition is a kind of electron transition mode existing in many metal−ligand inorganic complexes and organic molecules. A charge-transfer complex consists of an electron donor group bonded to an electron acceptor. When the complex absorbs radiation, an electron from the donor is transferred to an orbital that is largely associated with the acceptor. The excited state is thus the product of a kind of internal oxidation−reduction process.[18] Generally, nitrogen groups (which have lone pair electrons) often act as the electron donor, and aromatics act as the acceptor (Figure 5a),[19] and accordingly, the charge carrier excitation and recombination process is given in Figure 5b. Under light illumination, the electrons on the HOMO of nitrogen-related groups will be excited to the LUMO of quinoline groups (Figure 5c). In fact, similar photoexcitation pathways can be found in the interface of semiconductor/semiconductor and semiconductor/dye, which is the so-called interfacial charge-transfer transition.[20] With more quinoline rings being incorporated, the absorption edges located at long wavelength gradually red-shift, indicating the narrowed gap between the HOMO of the donor and the LUMO of the acceptor (Figure S7).

Photoluminescence (PL) spectra of all the samples, as shown in Figure 4b, exhibit two distinguishing PL bands/shoulder bands. The band at the shorter wavelength of around 440 nm for all the samples is attributed to the intrinsic LUMO-to-HOMO emission of carbon nitride, which corresponds to their slightly different band gaps. The other PL band results from charge transfer emission (Figure 5d). This representative dual-band optical absorption/PL spectrum can also be found in other donor−acceptor polymers.[21] From CN to CNQ-0.50, this band gradually red-shifts, which is in agreement with the UV−vis absorption spectra. Note that a weak shoulder band at around 463 nm, which is attributed to charge transfer emission, also appears in the PL spectrum of CN. We believe that in CN, the electron donor and acceptor are the tertiary nitrogen and 3,s-triazine ring, respectively (Figure S8a). Because of the low electron affinity of the 3,s-triazine ring (high LUMO), charge transfer transition in CN (Figure S8b) is less likely to happen

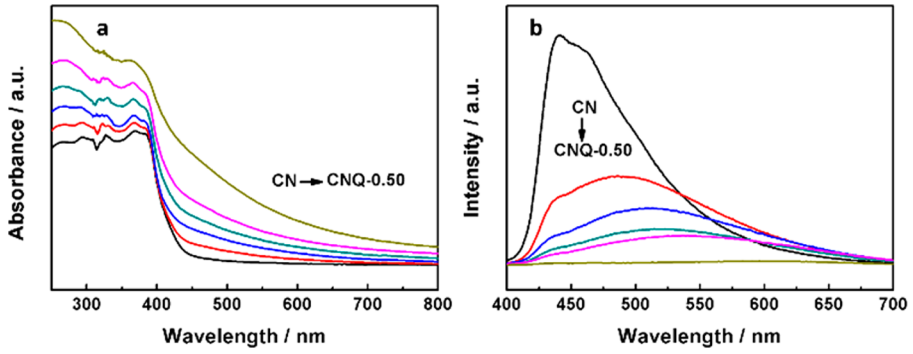

Figure 4. (a) UV−vis absorption spectra and (b) PL spectra (excitation wavelength=380 nm) of all the samples prepared.

DOI: 10.1021/acscatal.5b01155
ACS Catal. 2015, 5, 5008−5015

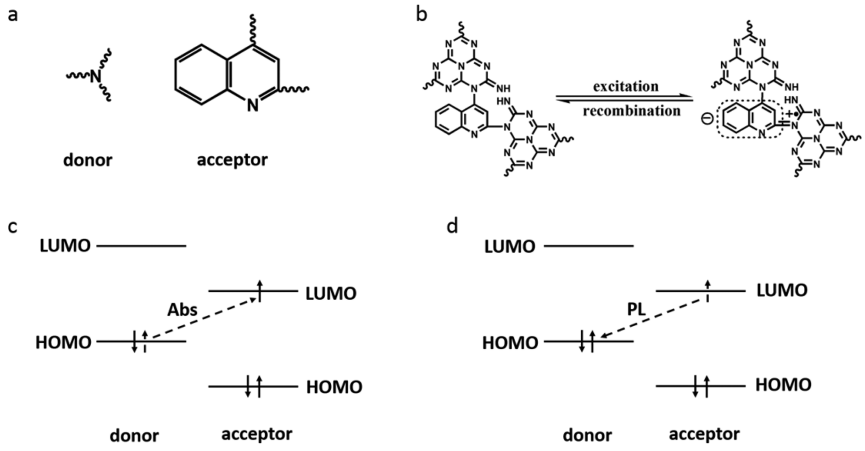

Figure 5. Schematics of (a) electron donor and acceptor, (b) charge carrier excitation and recombination, (c) charge transfer transition, and (d) photoluminescence (PL) path in quinoline-incorporated g-C_3N_4.

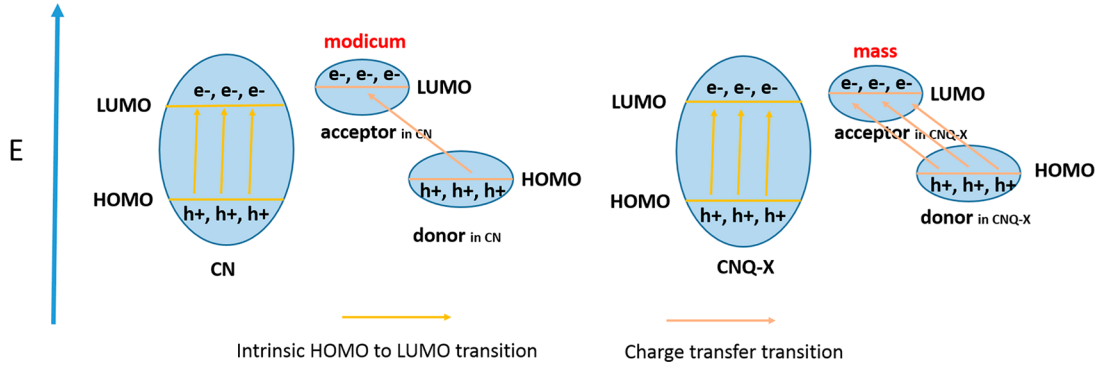

Figure 6. Diagram of the two electron transition modes in CN and CNQ-*X*.

compared with CNQ-*X*s, in which the electron acceptor (quinoline ring) is more apt to accept electrons. So the number of photoinduced electrons located at the acceptor in CNQ-*X*s are much more than that in CN. Figure 6 gives the diagram of the two electron transition modes occurring in CN and CNQ-*X*. It can be seen in Figure 4b that the intensity of the PL bands exhibit a significant decrease with the increasing incorporation of quinoline rings. Generally speaking, compared with the rigid planar structure of CN, the distorted structure of CNQ-*X*s means an increased probability of intramolecular collision, which will result in an energy loss of excitons and fluorescence quenching.

CN and CNQ-0.03 were selected to conduct time-resolved fluorescence decay spectra (Figure S9). Deconvolution of these spectra gives three radiative lifetimes as listed in Table 1.[22] For

Table 1. Radiative Fluorescence Lifetimes and Their Relative Percentages of CN and CNQ-0.03 Monitored at Different Wavelengths

sample	λ, nm	τ_1, ns, rel %	τ_2, ns, rel %	τ_3, ns, rel % (τ_{3v}[c] ns)
CN	440[a]	2.64–55.21	7.90–35.06	24.85–9.73 (2.42)
	463[b]	1.99–40.78	6.90–44.44	29.59–14.78 (4.37)
CNQ-0.03	436[a]	0.43–38.13	2.08–41.92	7.37–19.95 (1.47)
	510[b]	0.78–23.11	3.69–50.75	12.24–26.14 (3.20)

[a]Intrinsic LUMO-to-HOMO fluorescence emission. [b]Charge transfer fluorescence emission. τ1, τ2, τ3 can represent the longevity of short-lived, medial-lived, and long-lived carriers, respectively. [c]The total longevity of long-lived charge carriers (= τ_3 × rel %).

both samples, the percentage and longevity of long-lived charge carriers due to charge transfer fluorescence emission are higher than that caused by intrinsic LUMO-to-HOMO fluorescence emission. Such a longevity difference between these two excitation modes can be related to the relative positions of photoinduced holes and electrons. In the intrinsic HOMO-to-LUMO transition, the photoinduced holes and electrons are in the identical 3,s-triazine ring (h^+ mainly locates on N, and e^-, on C),[8] so they tend to recombine with each other with a high probability. However, the h^+ and e^- locate at two separate groups (N and aromatic ring, respectively) in the case of charge transfer transition. The photoinduced electrons can be much more strongly delocalized and remain stable at aromatic rings, thus mitigating the recombination with photogenerated holes. This test proves that, compared with the photoinduced electrons excited from an intrinsic HOMO-to-LUMO transition, the electrons generated from a charge transfer transition are more difficult to recombine with the holes and, consequently, it is more probable that they will take part in photochemical reactions. In addition, it can be seen that the ratio of (the longevity of long-lived charge carriers due to charge transfer fluorescence emission)/(the longevity of long-lived charge carriers due to intrinsic HOMO-to-LUMO transition) (3.20/1.47 = 2.18) in CNQ-0.03 is significantly higher than that for CN (4.37/2.42 = 1.81), which demonstrates that the charge transfer transition plays a more dominant role in CNQ-0.03.

The hydrogen evolution activities of CN and CNQ-*X*s are presented in Figure 7a. It can be seen that the hydrogen

DOI: 10.1021/acscatal.5b01155
ACS Catal. 2015, 5, 5008–5015

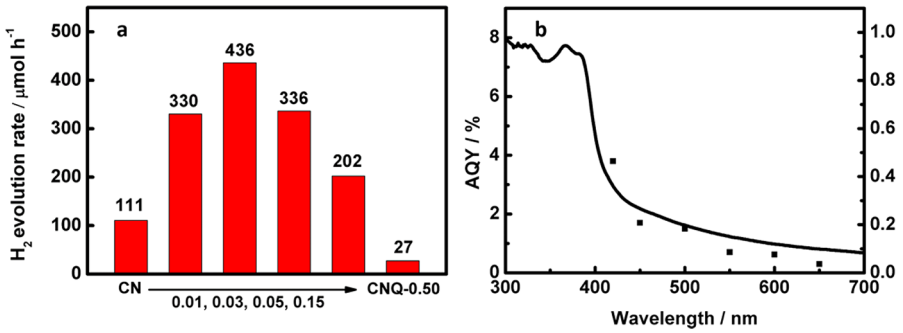

Figure 7. (a) Hydrogen evolution rates of CN and CNQ-*X*s and (b) wavelength-dependent apparent quantum yield of CNQ-0.03.

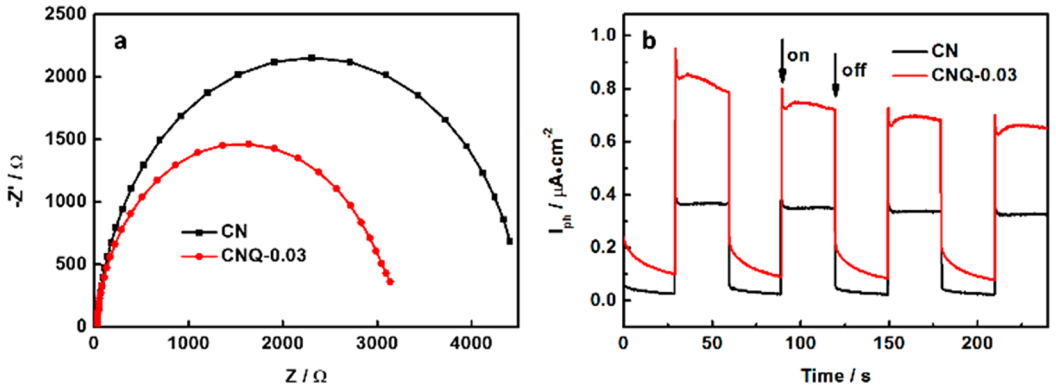

Figure 8. Photoelectrochemical properties of CN and CNQ-0.03. (a) Electrochemical impedance spectroscopy Nyquist plots in the dark and (b) periodic on/off photocurrent response under visible-light irradiation.

evolution activity has been largely enhanced by incorporating a moderate amount of quinoline rings into g-C_3N_4 networks. CNQ-0.03 shows the highest hydrogen evolution activity (436 μmol h^{-1}, 0.1 g catalyst), which is among one of the most excellent g-C_3N_4-based hydrogen evolution photocatalysts[13,23] and remarkably superior to an excellent visible-light photocatalyst such as black titania (140 μmol h^{-1} g^{-1})[24a,b] and N-doped black titania (200 μmol h^{-1} g^{-1}).[24c] Furthermore, as shown in Figure S10, CNQ-0.03 shows good photostability. Its wavelength-dependent apparent quantum yield (AQY) is shown in Figure 7b. The wavelength dependence of the AQY almost matches with the optical absorption spectrum. According to the traditional band theory, which used to guide inorganic heterogeneous photocatalytic research, only when the wavelength of incident light is shorter than a certain threshold (λ = 1240/band gap) could the photogenerated electrons and holes be induced in semiconductors and the photocatalytic reactions be initiated. Special attention should be paid to the active wavelength of CNQ-0.03: it is as long as 650 nm, which is much longer than its theoretical excitation wavelength (1240/2.94 = 422 nm). This disobeys the traditional perspective. Actually, a similar phenomenon has also been observed in pristine g-C_3N_4[8,12b] and other modified g-C_3N_4 photocatalysts,[11a,13,25] but has not drawn any researchers' attention, and no explanation has been given. Here, by employing the intramolecular charge transfer transition as described in this paper, we can give a satisfactory explanation on this phenomenon. The previous paragraph mentioned that intramolecular charge transfer transition can happen in pristine g-C_3N_4 (Figure S8), in which nitrogen groups act as the electron donor while 3,s-triazine units act as the acceptor. The smaller gap (between the HOMO of the donor and the LUMO of the acceptor) than the intrinsic band gap makes it possible for pristine g-C_3N_4 to absorb long-wavelength light. Tuning the energy level of a pristine acceptor (3,s-triazine units)[11a,13,25] or introducing a new acceptor into carbon nitride networks (this work) can further extend the active wavelength. This finding is very beneficial for understanding the photocatalytic performance of g-C_3N_4 under long-wavelength-light irradiation.

It is acknowledged that the hydrogen evolution activity of a semiconductor is determined by its surface area, energy level of the photoinduced electrons, band gap width, and the separation efficiency of the charge carriers. Generally speaking, a larger surface area means more catalytic active sites and a higher catalytic activity. It can be seen in Figure S11 that the BET surface area ratio and H_2 production rate ratio share a similar evolution trend, with an increase in CN(Q-*X*s)/CN, proving that a larger surface area would make some contributions to the photocatalytic performance enhancement. However, the normalized hydrogen evolution rate with respect to the specific surface area (H_2 evolution rate ratio/BET surface area ratio) is considerably high than 100% (except CNQ-0.50), suggesting that the surface area can hardly play a decisive role in these photocatalytic systems.[25b] By performing the valence band X-ray photoelectron spectroscopy,[26] the intrinsic HOMO energy level of CN and CNQ-0.03 were estimated to be 2.08 and 2.06 eV (Figure S12), respectively. Considering the band gap widths of CN (2.93 eV) and CNQ-0.03 (2.94 eV), the LUMO energy level of CNQ-0.03 is increased by only 0.03 eV compared with CN, so the photoinduced electrons located at the respective intrinsic LUMO positions have little influence on their huge difference of photocatalytic performance. As above-mentioned, the number of photoinduced electrons located at the acceptor

DOI: 10.1021/acscatal.5b01155
ACS Catal. 2015, 5, 5008−5015

in CNQ-0.03 are much more than that in CN. Meanwhile, these photoinduced electrons in CNQ-*X*s locate at a higher energy level compared with the photoinduced electrons located at their intrinsic LUMOs (Figure S13), which endows CNQ-0.03 with a larger driving force than CN to initiate reduction reaction.

In Figure 8a, an obvious decrease in semicircular Nyquist plots is observed for CNQ-0.03 in the dark, demonstrating that the incorporating motifs in carbon nitride networks can effectively improve the electronic conductivity of the polymer matrix.[13] This result is confirmed by the photocurrent measurements (Figure 8b), which show an enhancement in the I_{ph} of CNQ-0.03 over CN.[13] The incorporation of quinoline rings obviously facilitates charge transfer and separation. With more quinoline rings being incorporated, the LUMO energy level of the acceptor gradually become lower, which partially accounts for the gradually decreased hydrogen evolution activity of CNQ-*X*s. Moreover, because of the gradually distorted structure, more energy of the photogenerated electrons will dissipate in the forms of vibrational/thermal energy, etc., which is also responsible for the decreased photocatalytic activity at excessive amounts of quinoline ring incorporation.

To verify the universality of this modification strategy, a series of other fundamental aromatic rings, including benzene, pyridine, and pyrimidine, were incorporated into carbon nitride networks. Carbon nitride polymers including these aromatic rings all show enhanced hydrogen evolution activity (Figure 9).

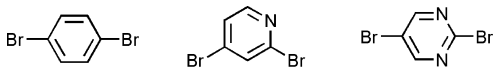

170(1) 313 (1) 301 (0.03)

Figure 9. Employed monomers for constructing donor−acceptor carbon nitride photocatalysts. The numbers in the parentheses are the dosages of monomer (g). The numbers outside the parentheses represent the corresponding hydrogen evolution rates (μmol h^{-1}).

Investigation of this is in progress. The optimized dosages of bromo aromatic compounds are mainly determined by their volatility, thermal stability, nucleophilic substitution activity, the electron affinity, and the permitted electron delocalization range of their corresponding aromatic rings. By selecting or designing appropriate aromatic rings, more efficient donor−acceptor conjugated photocatalysts based on carbon nitride can be expected.

4. CONCLUSIONS

Various intramolecular donor−acceptor conjugated copolymers were successfully constructed by incorporating aromatic rings into g-C_3N_4 networks, and the visible light absorbance and charge carrier separation/mobility of the polymer have been remarkably enhanced. The intramolecular charge transfer transition from the HOMO of donor (N) to the LOMO of acceptor (aromatic ring) is believed to play a significant role in their remarkably improved hydrogen evolution activity. In light of this concept, not limited to carbon nitride, various kinds of other intramolecular donor−acceptor polymers for photocatalytic reactions can be designed. More importantly, the photocatalytic mechanism proposed in this paper is applicable to explaining the photocatalytic activity of (pure or modified) g-C_3N_4 under long-wavelength-light irradiation, which has not been discussed before. The present findings provide beneficial experimental and theoretical guidance for the design of highly efficient polymeric photocatalysts.

■ ASSOCIATED CONTENT

Supporting Information

The Supporting Information is available free of charge on the ACS Publications website at DOI: 10.1021/acscatal.5b01155.

Relevant figures and tables as noted in the text (PDF)

■ AUTHOR INFORMATION

Corresponding Authors

*E-mail: zhlingxia@mail.sic.ac.cn.
*E-mail: jlshi@mail.sic.ac.cn.

Notes

The authors declare no competing financial interest.

■ ACKNOWLEDGMENTS

The authors gratefully acknowledge financial support from National Key Basic Research Program of China (2013CB933200), National 863 plans projects (2012AA062703), National Natural Science Foundation of China (Grant No. 21177137), and Science and Technology Commission of Shanghai Municipality (11JC1413400). The authors thank Dr. Rong Qian for help in the FT-IR measurements.

■ REFERENCES

(1) Armaroli, N.; Balzani, V. *Angew. Chem., Int. Ed.* **2007**, *46*, 52−66.
(2) (a) Lewis, N. S.; Nocera, D. G. *Proc. Natl. Acad. Sci. U.S.A.* **2006**, *103*, 15729−15735. (b) Kamat, P. V. *J. Phys. Chem. C* **2007**, *111*, 2834−2860.
(3) (a) Gratzel, M. *Nature* **2001**, *414*, 338−344. (b) Günes, S.; Neugebauer, H.; Sariciftci, N. S. *Chem. Rev.* **2007**, *107*, 1324−1338. (c) Huynh, W. U.; Dittmer, J. J.; Alivisatos, A. P. *Science* **2002**, *295*, 2425−2427. (d) Wang, Y.; Wang, X.; Antonietti, M. *Angew. Chem., Int. Ed.* **2012**, *51*, 68−89. (e) Schwinghammer, K.; Tuffy, B.; Mesch, M. B.; Wirnhier, E.; Martineau, C.; Taulelle, F.; Schnick, W.; Senker, J.; Lotsch, B. V. *Angew. Chem., Int. Ed.* **2013**, *52*, 2435−2439.
(4) (a) Asahi, R.; Morikawa, T.; Ohwaki, T.; Aoki, K.; Taga, Y. *Science* **2001**, *293*, 269−271. (b) Maeda, K.; Teramura, K.; Lu, D.; Takata, T.; Saito, N.; Inoue, Y.; Domen, K. *Nature* **2006**, *440*, 295−295. (c) Tsuji, I.; Kato, H.; Kobayashi, H.; Kudo, A. *J. Am. Chem. Soc.* **2004**, *126*, 13406−13413. (d) Wang, M.; Ioccozia, J.; Sun, L.; Lin, C.; Lin, Z. *Energy Environ. Sci.* **2014**, *7*, 2182−2202. (e) Ye, M.; Gong, J.; Lai, Y.; Lin, C.; Lin, Z. *J. Am. Chem. Soc.* **2012**, *134*, 15720−15723.
(5) (a) Kohler, A.; dos Santos, D. A.; Beljonne, D.; Shuai, Z.; Bredas, J. L.; Holmes, A. B.; Kraus, A.; Mullen, K.; Friend, R. H. *Nature* **1998**, *392*, 903−906. (b) Liang, Y.; Yu, L. *Acc. Chem. Res.* **2010**, *43*, 1227−1236.
(6) (a) Brédas, J. L.; Beljonne, D.; Coropceanu, V.; Cornil, J. *Chem. Rev.* **2004**, *104*, 4971−5004. (b) Jenekhe, S. A.; Lu, L.; Alam, M. M. *Macromolecules* **2001**, *34*, 7315−7324.
(7) (a) Yu, G.; Gao, J.; Hummelen, J. C.; Wudl, F.; Heeger, A. J. *Science* **1995**, *270*, 1789−1791. (b) Park, S. H.; Roy, A.; Beaupré, S.; Cho, S.; Coates, N.; Moon, J. S.; Moses, D.; Leclerc, M.; Lee, K.; Heeger, A. J. *Nat. Photonics* **2009**, *3*, 297−302. (c) Roquet, S.; Cravino, A.; Leriche, P.; Alévêque, O.; Frère, P.; Roncali, J. *J. Am. Chem. Soc.* **2006**, *128*, 3459−3466. (d) Wang, M.; Hu, X.; Liu, P.; Li, W.; Gong, X.; Huang, F.; Cao, Y. *J. Am. Chem. Soc.* **2011**, *133*, 9638−9641. (e) Chang, Y.-T.; Hsu, S. L.; Su, M.-H.; Wei, K.-H. *Adv. Mater.* **2009**, *21*, 2093−2097.
(8) (a) Wang, X.; Maeda, K.; Thomas, A.; Takanabe, K.; Xin, G.; Carlsson, J. M.; Domen, K.; Antonietti, M. *Nat. Mater.* **2009**, *8*, 76−80.

DOI: 10.1021/acscatal.5b01155
ACS Catal. 2015, 5, 5008−5015

(b) Liu, J.; Liu, Y.; Liu, N.; Han, Y.; Zhang, X.; Huang, H.; Lifshitz, Y.; Lee, S.; Zhong, J.; Kang, Z. *Science* **2015**, *347*, 970−974.
(9) (a) Yanagida, S.; Kabumoto, A.; Mizumoto, K.; Pac, C.; Yoshino, K. *J. Chem. Soc., Chem. Commun.* **1985**, 474−475. (b) Matsuoka, S.; Kohzuki, T.; Nakamura, A.; Pac, C.; Yanagida, S. *J. Chem. Soc., Chem. Commun.* **1991**, 580−581. (c) Yamamoto, T. *Prog. Polym. Sci.* **1992**, *17*, 1153−1205. (d) Shibata, T.; Kabumoto, A.; Shiragami, T.; Ishitani, O.; Pac, C.; Yanagida, S. *J. Phys. Chem.* **1990**, *94*, 2068−2076. (e) Maruyama, T.; Yamamoto, T. *J. Phys. Chem. B* **1997**, *101*, 3806−3810. (f) Zhang, Z.; Long, J.; Yang, L.; Chen, W.; Dai, W.; Fu, X.; Wang, X. *Chem. Sci.* **2011**, *2*, 1826−1830.
(10) (a) Wang, X.; Blechert, S.; Antonietti, M. *ACS Catal.* **2012**, *2*, 1596−1606. (b) Zheng, Y.; Liu, J.; Liang, J.; Jaroniec, M.; Qiao, S. *Energy Environ. Sci.* **2012**, *5*, 6717−6731. (c) Zhao, Z.; Sun, Y.; Dong, F. *Nanoscale* **2015**, *7*, 15−37.
(11) (a) Li, X. H.; Chen, J. S.; Wang, X.; Sun, J.; Antonietti, M. *J. Am. Chem. Soc.* **2011**, *133*, 8074−8077. (b) Zhang, J.; Zhang, M.; Sun, R. Q.; Wang, X. *Angew. Chem., Int. Ed.* **2012**, *51*, 10145−10149. (c) Li, X. H.; Baar, M.; Blechert, S.; Antonietti, M. *Sci. Rep.* **2013**, *3*, 1743. (d) Hou, Y.; Laursen, A. B.; Zhang, J.; Zhang, G.; Zhu, Y.; Wang, X.; Dahl, S.; Chorkendorff, I. *Angew. Chem., Int. Ed.* **2013**, *52*, 3621−3625. (d) Hou, Y.; Wen, Z.; Cui, S.; Guo, X.; Chen, J. *Adv. Mater.* **2013**, *25*, 6291−6297. (e) Li, X. H.; Antonietti, M. *Chem. Soc. Rev.* **2013**, *42*, 6593−6604. (f) Cai, Y. Y.; Li, X. H.; Zhang, Y. N.; Wei, X.; Wang, K. X.; Chen, J. S. *Angew. Chem., Int. Ed.* **2013**, *52*, 11822−11825. (g) Li, X. H.; Cai, Y. Y.; Gong, L. H.; Fu, W.; Wang, K. X.; Bao, H. L.; Wei, X.; Chen, J. S. *Chem. - Eur. J.* **2014**, *20*, 16732−16737. (h) Sun, L.; Qi, Y.; Jia, C. J.; Jin, Z.; Fan, W. *Nanoscale* **2014**, *6*, 2649−2659. (k) Guo, L. T.; Cai, Y. Y.; Ge, J. M.; Zhang, Y. N.; Gong, L. H.; Li, X. H.; Wang, K. X.; Ren, Q. Z.; Su, J.; Chen, J. S. *ACS Catal.* **2015**, *5*, 388−392.
(12) (a) Liu, J.; Zhang, T.; Wang, Z.; Dawson, G.; Chen, W. *J. Mater. Chem.* **2011**, *21*, 14398−14401. (b) Zhang, G.; Zhang, J.; Zhang, M.; Wang, X. *J. Mater. Chem.* **2012**, *22*, 8083−8091.
(13) (a) Zhang, J.; Zhang, G.; Chen, X.; Lin, S.; Mohlmann, L.; Dolega, G.; Lipner, G.; Antonietti, M.; Blechert, S.; Wang, X. *Angew. Chem., Int. Ed.* **2012**, *51*, 3183−3187. (b) Zhang, G.; Wang, X. *J. Catal.* **2013**, *307*, 246−253. (c) Zhang, J.; Zhang, M.; Lin, S.; Fu, X.; Wang, X. *J. Catal.* **2014**, *310*, 24−30. (d) Zhang, M.; Wang, X. *Energy Environ. Sci.* **2014**, *7*, 1902−1906.
(14) Bandyopadhyay, S.; Massoth, F. E.; Pons, S.; Eyring, E. M. *J. Phys. Chem.* **1985**, *89*, 2560−2564.
(15) Jones, C.; Sammann, E. *Carbon* **1990**, *28*, 509−514.
(16) Hong, Z.; Shen, B.; Chen, Y.; Lin, B.; Gao, B. *J. Mater. Chem. A* **2013**, *1*, 11754−11761.
(17) Chen, X.; Shen, S.; Guo, L.; Mao, S. S. *Chem. Rev.* **2010**, *110*, 6503−6570.
(18) Skoog, D. A.; Holler, F. J.; Crouch, S. R. *Principles of Instrumental Analysis*, 6th ed.; Thomson-Brooks/Cole: Belmont, CA, USA, 2006, 371−371.
(19) Grabowski, Z. R.; Rotkiewicz, K.; Rettig, W. *Chem. Rev.* **2003**, *103*, 3899−4031.
(20) (a) Bledowski, M.; Wang, L.; Ramakrishnan, A.; Khavryuchenko, O. V.; Khavryuchenko, V. D.; Ricci, P. C.; Strunk, J.; Cremer, T.; Kolbeck, C.; Beranek, R. *Phys. Chem. Chem. Phys.* **2011**, *13*, 21511−21519. (b) Creutz, C.; Brunschwig, B. S.; Sutin, N. *J. Phys. Chem. B* **2005**, *109*, 10251−10260. (c) Creutz, C.; Brunschwig, B. S.; Sutin, N. *J. Phys. Chem. B* **2006**, *110*, 25181−25190. (d) Duncan, W. R.; Prezhdo, O. V. *Annu. Rev. Phys. Chem.* **2007**, *58*, 143−184. (e) Macyk, W.; Szaciłowski, K.; Stochel, G.; Buchalska, M.; Kuncewicz, J.; Łabuz, P. *Coord. Chem. Rev.* **2010**, *254*, 2687−2701.
(21) (a) Gibson, G. L.; McCormick, T. M.; Seferos, D. S. *J. Am. Chem. Soc.* **2012**, *134*, 539−547. (b) Jenekhe, S.; Lu, L.; Alam, M. *Macromolecules* **2001**, *34*, 7315−7324. (c) Kulkarni, A.; Zhu, Y.; Babel, A.; Wu, P.; Jenekhe, S. *Chem. Mater.* **2008**, *20*, 4212−4223.
(22) (a) Niu, P.; Liu, G.; Cheng, H. *J. Phys. Chem. C* **2012**, *116*, 11013−11018. (b) Niu, P.; Zhang, L.; Liu, G.; Cheng, H. *Adv. Funct. Mater.* **2012**, *22*, 4763−4770.
(23) (a) Sun, J.; Zhang, J.; Zhang, M.; Antonietti, M.; Fu, X.; Wang, X. *Nat. Commun.* **2012**, *3*, 1139. (b) Lin, Z.; Wang, X. *Angew. Chem., Int. Ed.* **2013**, *52*, 1735−1738. (c) Yang, S.; Gong, Y.; Zhang, J.; Zhan, L.; Ma, L.; Fang, Z.; Vajtai, R.; Wang, X.; Ajayan, P. M. *Adv. Mater.* **2013**, *25*, 2452−2456. (d) Zheng, Y.; Lin, L.; Ye, X.; Guo, F.; Wang, X. *Angew. Chem., Int. Ed.* **2014**, *53*, 11926−11930.
(24) (a) Chen, X.; Liu, L.; Yu, P. Y.; Mao, S. S. *Science* **2011**, *331*, 746−750. (b) Wang, Z.; Yang, C.; Lin, T.; Yin, H.; Chen, P.; Wan, D.; Xu, F.; Huang, F.; Lin, J.; Xie, X.; Jiang, M. *Energy Environ. Sci.* **2013**, *6*, 3007−3014. (c) Lin, T.; Yang, C.; Wang, Z.; Yin, H.; Lü, X.; Huang, F.; Lin, J.; Xie, X.; Jiang, M. *Energy Environ. Sci.* **2014**, *7*, 967−972.
(25) (a) Wang, X.; Maeda, K.; Chen, X.; Takanabe, K.; Domen, K.; Hou, Y.; Fu, X.; Antonietti, M. *J. Am. Chem. Soc.* **2009**, *131*, 1680−1681. (b) Liu, G.; Niu, P.; Sun, C.; Smith, S.; Chen, Z.; Lu, G.; Cheng, H. *J. Am. Chem. Soc.* **2010**, *132*, 11642−11648. (c) Schwinghammer, K.; Tuffy, B.; Mesch, M.; Wirnhier, E.; Martineau, C.; Taulelle, F.; Schnick, W.; Senker, J.; Lotsch, B. *Angew. Chem., Int. Ed.* **2013**, *52*, 2435−2439. (d) Bhunia, M.; Yamauchi, K.; Takanabe, K. *Angew. Chem., Int. Ed.* **2014**, *53*, 11001−11005. (e) Zhang, G.; Zhang, M.; Ye, X.; Qiu, X.; Lin, S.; Wang, X. *Adv. Mater.* **2014**, *26*, 805−809.
(26) (a) Liu, G.; Wang, L.; Sun, C.; Yan, X.; Wang, X.; Chen, Z.; Smith, S.; Cheng, H.; Lu, G. *Chem. Mater.* **2009**, *21*, 1266−1274. (b) Liu, G.; Niu, P.; Yin, L.; Cheng, H. *J. Am. Chem. Soc.* **2012**, *134*, 9070−9073.

DOI: 10.1021/acscatal.5b01155
ACS Catal. 2015, 5, 5008−5015